CEE361 Final Project - Linear elastic fracture mechanics with FEM

Alex Chang, Kevin Park

Motivation

Finite element methods (FEM) are often used in engineering applications due to the difficulties associated with finding strong form solutions to complex models. The computational feasibility of FEM comes with tradeoffs, however – due to their discrete nature, FEM-derived solutions can suffer from inaccuracies/imprecisions depending on the discretization scheme utilized to model a particular geometry.

These issues are particularly relevant in regions of structures with localized stress concentrations, such as that of the crack tip in a fractured block. In such cases, stress concentrations may vary significantly in a dense location, requiring more detailed discretization/meshing techniques to guarantee accurate modelling. By making this adjustment, finite element analysis (FEA) can be used for accurate crack analysis. FEA has its limitations within this domain, however - it cannot be used to analyze extreme crack deformations or crack propagation (mostly just material failures), and it cannot be used with determination of minimizing energy (only the method of weighted residuals). Singularities, such as those at the crack tip, may also provide unrealistic stress values for specific mesh elements. Furthermore, a significant number of mesh elements may be needed at the crack tip to achieve decent results.

This final project involves an implementation of linear elastic fracture mechanics with constant strain triangles (CSTs) to better understand how different meshing schemes affect output quality in reference to analytical solutions for three separate situations. Once an adequate meshing scheme is found, experimentation based on how different structural material compositions affect stress distributions is analyzed for the point crack model.

Methods

To create the models and mesh used for each fracture situation, we used the software Gmsh. We simulated three different situations, each of which consisted of a 10x10 square with some sort of crack in it. The first situation was a point crack created by two lines coming to a point on the left side of the square provided by Professor Li. The second was a circular hole in the middle of the square. The third was a crack on the left side consisting of two parallel lines that come to a rounded half-circular point at the end, similar to the first situation. The circular crack was used to test the simple, analytic equation $\sigma_{max} = \sigma\left(1 + 2\sqrt{\frac{a}{\rho}}\right)$ where a is the characteristic crack length (half the crack length for a crack inside the material, the full crack length for a crack on the edge of the material), ρ is the radius of curvature of the crack, σ_{max} is

the max stress around the crack, and σ is the nominal stress in the piece. This equation asserts that stress is 3x the nominal stress at the edge of a circular crack (which is the location of the max). We also tested this equation with the semicircular crack with different values for a and ρ. The point crack was used to test more experimental equations for stress around a point crack, as well as the effect of a singularity on CST density and distance from the crack.

We scattered points around the crack to increase or decrease the mesh density in those areas in Gmsh, then meshed each structure for various different mesh densities. We used MATLAB to take these meshes and run FEM on them for an equal force pulling up on the top surface and down on the bottom surface of the square. A pin constraint was used on the bottom right and a roller was used on the top right corners to constrain the piece in the most minimal way possible according to the 321 method, or 21 method for 2D. The 21 method was used because our scenario is a rigid body under equilibrium load, with no full constraints. We therefore constrain one point in 2 dimensions, and a second point in 1 dimension in order to fully constrain the 3 degrees of freedom of the model with minimal effect on the analysis by constraining the fewest amount of points in the least impactful way.

Once we had the constraints, we could calculate the displacements of the nodes after calculating the global stiffness matrix from each CSTs' elemental stiffness matrix. The displacement was used to calculate the stress, which we could directly analyze. For easier visualization, we calculated the Von Mises stress to get a scalar quantity that we could compare to analytic equations and also view on a heat plot to get a good concept of the distribution of stresses in each situation.

We then changed the material of the structure around the crack by modifying Poisson's ratio and Young's modulus for the CSTs within a given distance of the crack tip to test the effects of different materials on fracture mechanics. Because the material is no longer homogenous, the equations are not easily applicable because nominal stress is taken in a different material than max stress.

Results

In order to visualize the stress distribution easier, a heat map with different colors corresponding to the Von Mises stress magnitude of each CST was implemented. A log scaling was applied to the stresses to make their distribution more uniform and thus readily apparent; otherwise, the color scaling of the heat map is extremely skewed towards lower values.

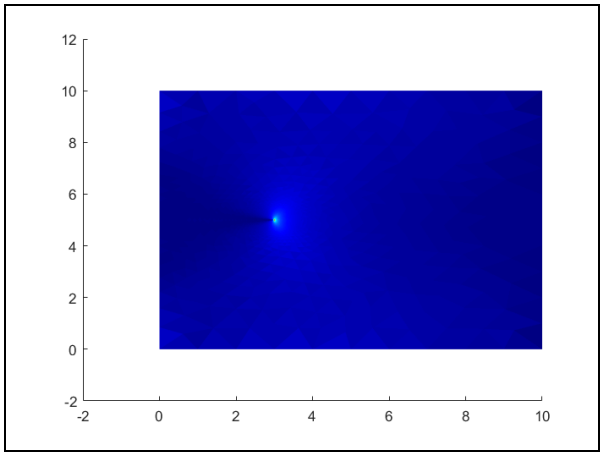

Figure 1: Point crack modelling without log scaling

With this modification, the relative quality of stress distributions based on meshing schemes can be analyzed. As mentioned in the motivation, higher CST counts are needed near highly variable stress concentrations to accurately model their distribution. The following figures for the point crack illustrate this problem, even though the lower CST counts exhibit the intuitive phenomena of a higher stress concentration at the crack tip. In comparison to denser meshes it is clear that the rate of stress increase approaching the crack tip is imprecise and the true min/max stress values are missing for the lower-resolution mesh – necessitating higher count meshes.

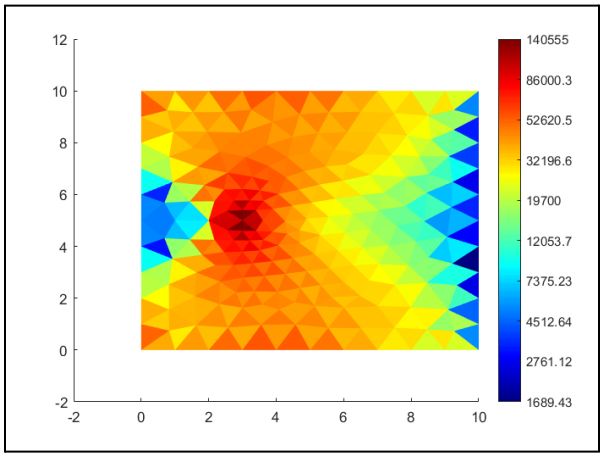

Figure 2: Point crack modelling with a low count of CSTs

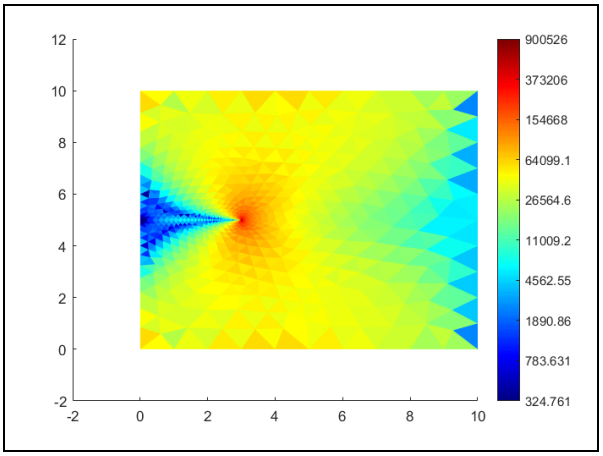

Figure 3: Point crack modelling with a medium count of CSTs

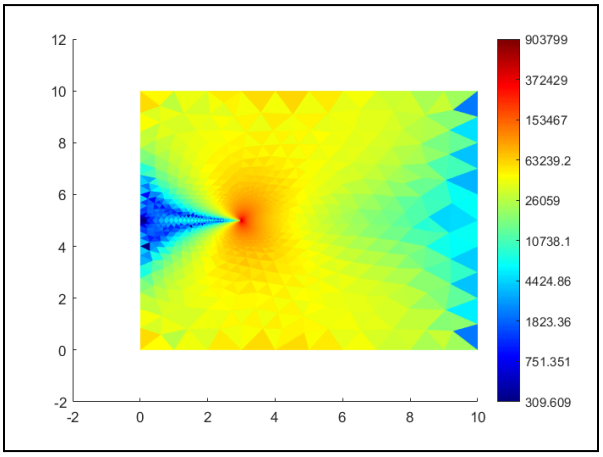

Figure 4: Point crack modelling with a high count of CSTs

Figure 2 has a relatively “broad” stress gradient in proximity to the crack tip, while Figure 3 and 4 have “tighter” gradients. Noticeably, the mins and maxs of the heatmap colorbar are also different; due to the constant strain of triangle elements, larger elements result in a loss of information. This can be improved by increasing element count such that individual elements shrink in size, approaching the continuous nature of physical real world materials.

The crack tip can also be analyzed using analytical equations that model stresses in its vicinity:

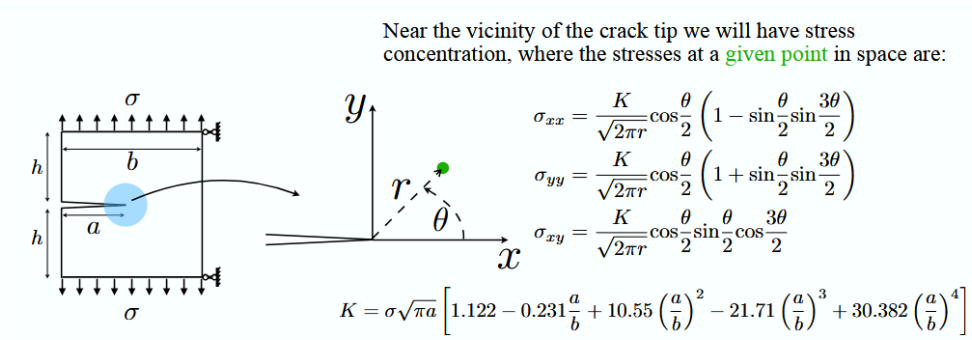

A function was implemented that prints a corresponding stress vector (σ_{xx}, σ_{yy}, $2\sigma_{xy}$) when an element is clicked. Several elements were selected and compared to analytical solutions, seen in Table # for the highest resolution mesh:

r (m)	***θ (rad)***	**FEA-derived (Pa)**	**Analytical (Pa)**
0.0297	0.9527	10^5*(3.0762, 4.7659, 0.9592)	10^5*(1.7201, 4.5797, 0.4082)
0.1698	0	10^5*(1.6455, 1.7013, -0.0685)	10^5*(1.4821, 1.4821, -0.0002)
0.1128	-1.4834	10^5*(0.6493, 2.4339, 0.6095)	10^5*(0.6221, 2.0593, 1.1025)
0.0460	0.5679	10^5*(2.8120, 3.6296, 0.7943)	10^5*(2.1579, 3.3107, 1.0090)

Table 1: High CST Density FEA-derived vs. analytical stress for a point crack

r (m)	***θ (rad)***	**FEA-derived (Pa)**	**Analytical (Pa)**
0.0276	1.0053	10^5*(1.7093, 3.7738, -0.3157)	10^5*(1.6722, 4.7691, 0.1950)
0.1703	0	10^5*(1.7179, 1.5146, 0.0800)	10^5*(1.4798, 1.4798, -0.0006)
0.1122	-1.4014	10^5*(0.6390, 3.1444, 0.6964)	10^5*(0.6190, 2.1683, 0.9106)
0.0430	0.6034	10^5*(1.8290, 4.4708, 0.6986)	10^5*(2.1559, 3.4711, 1.0327)

Table 2: Med CST Density FEA-derived vs. analytical stress for a point crack

r (m)	***θ (rad)***	**FEA-derived (Pa)**	**Analytical (Pa)**
0.0281	1.1227	10^5*(0.3762, 1.4464, 0.2615)	10^5*(1.4535, 4.7177, -0.3715)

0.1698	0	10^5*(9.7290, 8.4844, -2.6310)	10^5*(1.4821, 1.4821, -0.0002)
0.1128	-1.4834	10^5*(0.3762, 1.4463, -0.2626)	10^5*(0.6221, 2.0593, 1.1025)
0.0460	0.5679	10^5*(9.7260, 8.4545, 2.6332)	10^5*(2.1579, 3.3107, 1.0090)

Table 3: Low CST Density FEA-derived vs. analytical stress for a point crack

The circular and semicircular cracks can also be evaluated in a similar fashion with the analytical equation $\sigma_{max} = \sigma\left(1 + 2\sqrt{\frac{a}{\rho}}\right)$, using higher density meshes for greater accuracy. The FEA-derived and analytical max stresses, present at the crack edge, are listed in Table # for both models (seen in Figures 5 and 6):

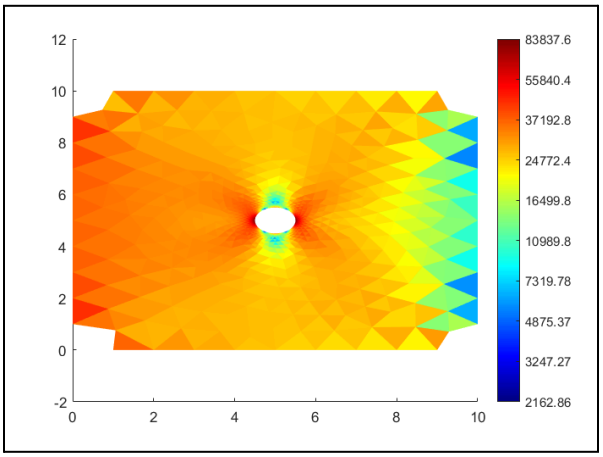

Figure 5: Circular crack modelling with a high count of CSTs

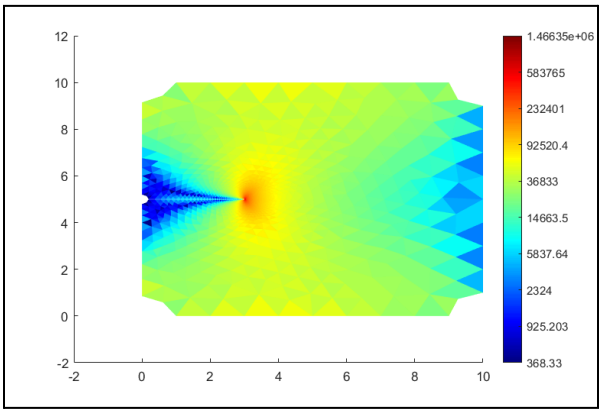

Figure 6: Semicircular crack modelling with a high count of CSTs

Case	FEA-derived max stress	Analytical max stress

Circular	83838	90000
Semicircular	1466350	1499693.8456699

Table 4: Max stresses derived from FEA and analytical solutions for circular and semicircular cracks

Returning to the point crack scenario, the effects of a composite material structure on stress distribution can be clearly seen in Figures 7-13. In these analyses, the Poisson's ratio and Young's modulus of CSTs within a box domain surrounding the crack tip were modified, using the highest mesh element count; the parameter changes are listed in the figure titles.

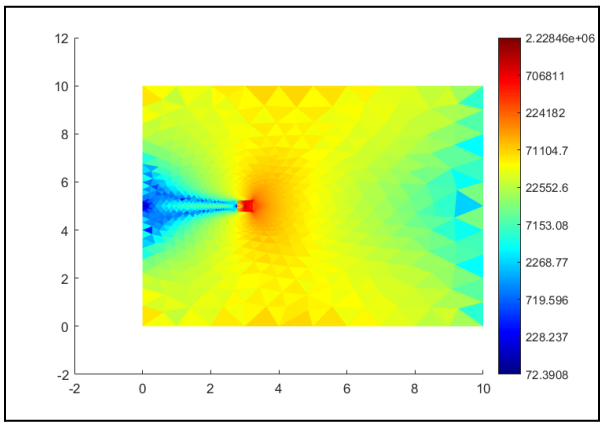

Figure 7: Composite crack for E = 10^5, ν = 0.1, box size = 0.5x0.5

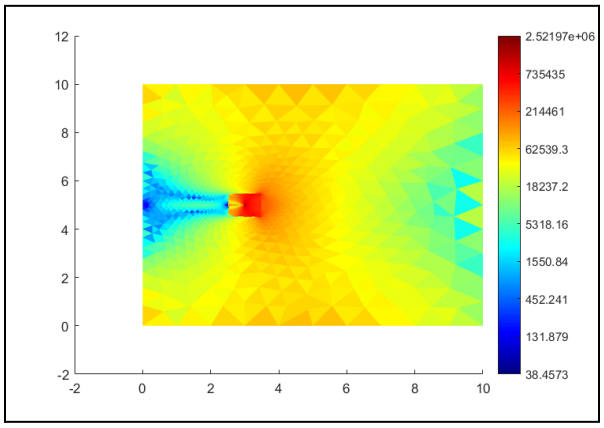

Figure 8: Composite crack for E = 10^5, ν = 0.1, box size = 1x1

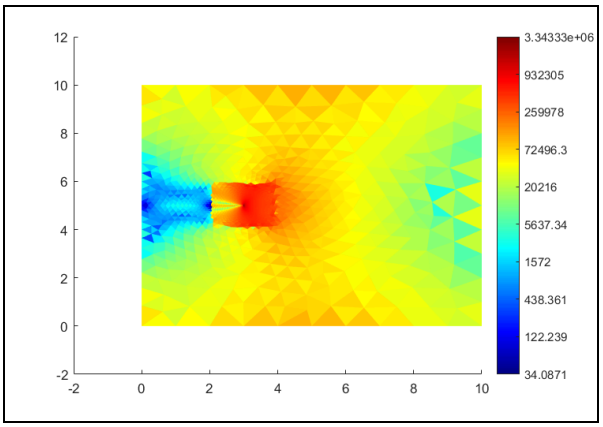

Figure 9: Composite crack for E = 10^5, ν = 0.1, box size = 2x2

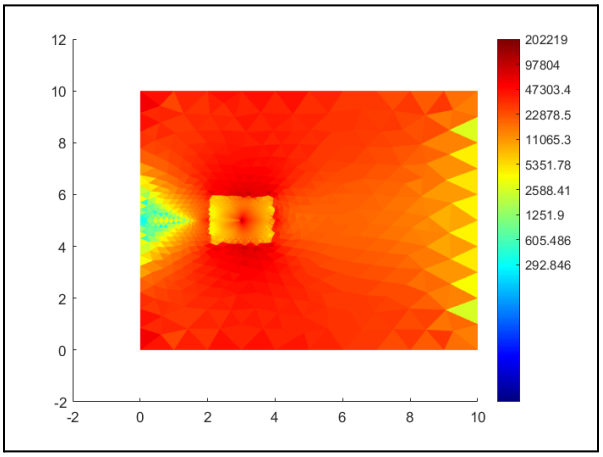

Figure 10: Composite crack for E = 10^{12}, ν = 0.1, box size = 2x2

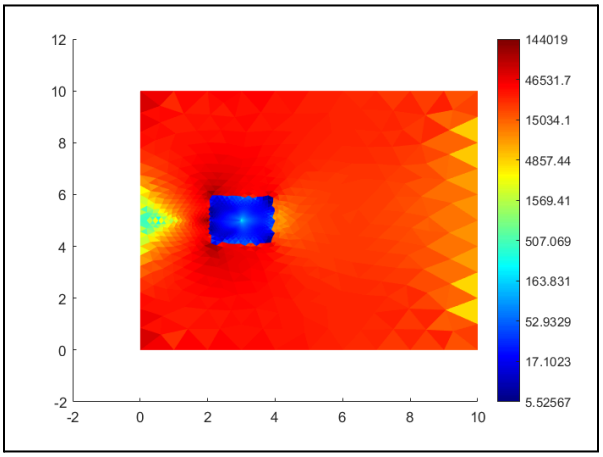

Figure 11: Composite crack for E = 10^{15}, ν = 0.1, box size = 2x2

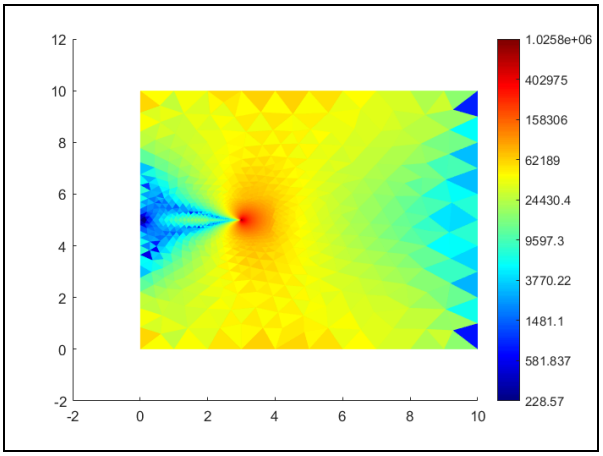

Figure 12: Composite crack for E = 10^{11}, ν = -0.5, box size = 2x2

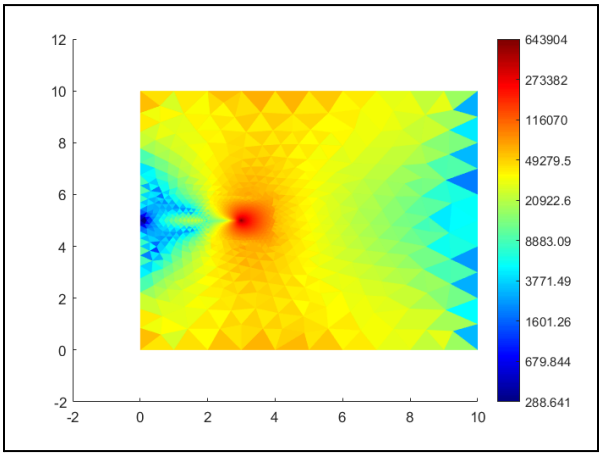

Figure 13: Composite crack for E = 10^{11}, ν = -0.99, box size = 2x2

Discussion/Conclusion

From our results it can be shown that FEM does converge to the analytic function $K = \sigma Y\sqrt{\pi a}$ with enough CSTs around a crack created by two straight lines. We calculated the stress analytically as a function of r and theta and compared it to our results from FEM. The stress based on the equation and based on FEM for the highest mesh count around the crack tip were very similar, but as less and less CSTs were used, the stress around the crack tip got smaller and smaller and thus farther from the analytic results. This is behavior the same as singularities in commercial FEA, as it is a fundamental part of FEM. Essentially, due to fracture mechanics, a crack with in infinitely small radius of curvature, or a sharp corner, will cause stress to go to infinity as you approach the crack tip. In real life, the material near the crack tip will undergo plastic deformation and blunt the tip, increasing the radius of curvature and preventing unrealistic infinite stress. However, in FEM, since plastic deformation is not implemented, the crack tip remains sharp and stress is extremely high near the crack. As you refine the mesh, the

triangles get closer to the crack tip, and therefore the stress in them increases dramatically, as we saw in our results.

For the circular meshes, the results were slightly different. We analyzed these situations using a different analytic equation to only analyze maximum stress. The results for this maximum stress were once again similar between FEM and analytic equations when the mesh was large enough, but grew more different as less CSTs were used. However, there were some issues in analyzing curved surfaces. Once circles were introduced into the mesh, the global stiffness matrix became near singular and MATLAB had a difficult time solving the linear equations. This resulted in NaN results for displacement for the four corners, leading to the gaps you see in the corners of the images for the circular and semicircular cracks. A super low mesh count for the circular hole was done to demonstrate this issue and can be seen in the appendix. Some possible causes of this issue could be ill-behaved CSTs on the circular element. Long and narrow CSTs are bad for stability, so the mesh was refined around the crack instead of just at the crack to help alleviate this, but the problem still persisted. Ill-behaved CSTs could still exist around the circle with near parallel edges or strange connections. Additionally, the constraints are minimal, and may cause the structure to be more unstable, so a combination of factors could cause the near-singularity of the stiffness matrix, but a concrete cause for this issue is still unknown. The matrix still calculates stresses on all areas but the two corners properly even with this behavior.

These results show promising use for FEM analysis of cracks in materials. For circular cracks, the results are promising since they approach the analytic values which are non-infinite, and therefore can be used to model realistic situations. The near-singularity of the stiffness matrix is an issue, however, that should be noted when modeling complex geometry or loosely constrained rigid bodies. Assuming a non-singular stiffness matrix, however, the results from FEM such as ours can be readily used for static analysis on real life parts and the results can be taken to be similar to real life results. For the point crack, it is harder to simply take stress values as truth, since plastic deformation will occur far before many of the values in the crack. The crack inevitably will round out due to the infinite stress at its tip, causing the geometry of the crack to change slightly and Y to be a different value. However, the results are still useful to check a binary question of whether the material will yield or not, since a result showing stresses far below yield around an appreciable area of the crack will be matched in real life. Stresses in the region of the crack but not extremely close to it can also be viewed as relatively accurate for lower stresses. Care still needs to be taken near all singularities or stresses above yield in FEM, and results must be carefully examined to determine if they are realistic before trusting FEM results.

Lastly, we analyzed the effects of composite materials on fracture mechanics. We changed the Poisson's ratio and Young's modulus around the crack in order to see how different

properties affected the stress concentrations, and we saw that stresses dramatically changed between materials with different properties, as expected. Lower Young's modulus near the crack caused higher stresses near the crack and higher Young's modulus caused lower stresses, which is to be expected. Additionally, higher Young's modulus composites had less stress and a smaller trail away from the crack tip towards the left, implying that the composite material holds the crack together better and less stress propagates away from the tip. The opposite is true for lower Young's modulus. Additionally, changing the poisson's ratio caused stress around the different material to be different. Higher Poisson's ratio contained the stress more and had lower maximum stress, while a lower Poisson's ratio that is still positive increased the maximum stress. This could be due to lower Poisson's ratios being less ductile and deforming less, causing more stress to be accumulated. Negative Poisson's ratios were also tested, with an extremely low value of -0.99 decreasing stress significantly, and a moderately negative value of -0.5 increasing stress. The increase in stress may be due to negative Poisson's ratio pulling the crack even farther apart as the plates separate. However, the decrease in stress for a theoretically possible -0.99 Poisson's ratio is much harder to explain. This type of material, however, does not occur naturally and is often made of complex geometries that may not be properly represented by FEM. Overall, this testing demonstrates that FEM confirms our intuition that stronger materials near the crack can reduce stress. However, one must be careful in using these results, as materials with high Young's modulus but low ultimate tensile strengths that are brittle may cause worse fracture resistance that cannot be represented by FEM. For example, infusing carbon into a steel part will make it stronger, but the added brittle nature can make it fail earlier when a large crack is introduced.

Our results demonstrate that FEM is a powerful tool for fracture mechanics that can accurately reproduce analytic results and give insight into the properties of materials with cracks in their geometry. By using a sufficient mesh density and number of CSTs, especially around cracks and areas with large stress gradients, accurate results can easily be obtained. However, as always with FEM, one must be careful with using its results as they must be interpreted properly and verified to be realistic. FEM does not account for situations such as plastic deformation, imperfections, or other real life properties, and therefore its results, while powerful, must be interpreted properly to be useful.

Appendix

Additional graphs of different meshing schemes and different point crack composite formulations can be seen below.

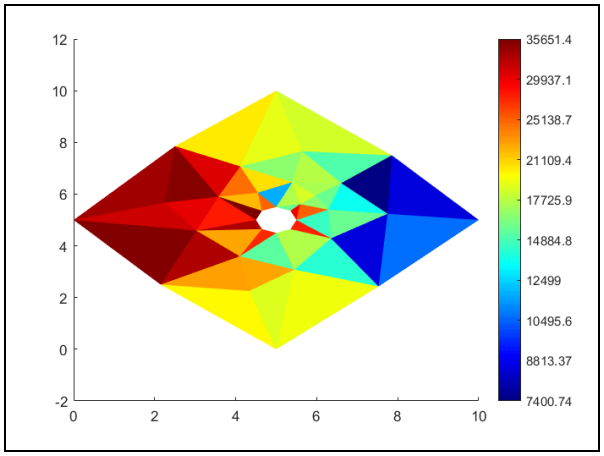

Figure 14: Circular crack modelling with a low count of CSTs

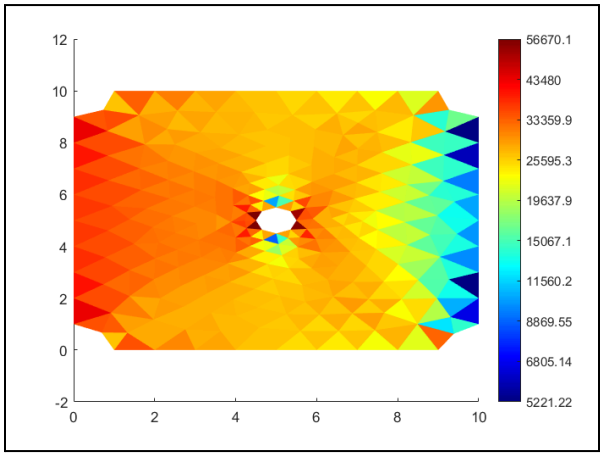

Figure 15: Circular crack modelling with a medium count of CSTs

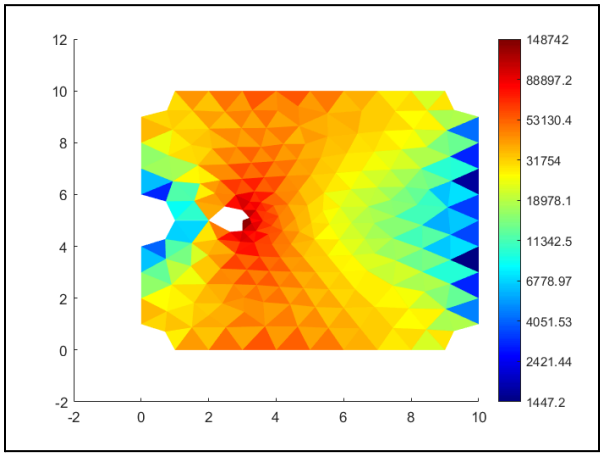

Figure 16: Semicircular crack modelling with a low count of CSTs

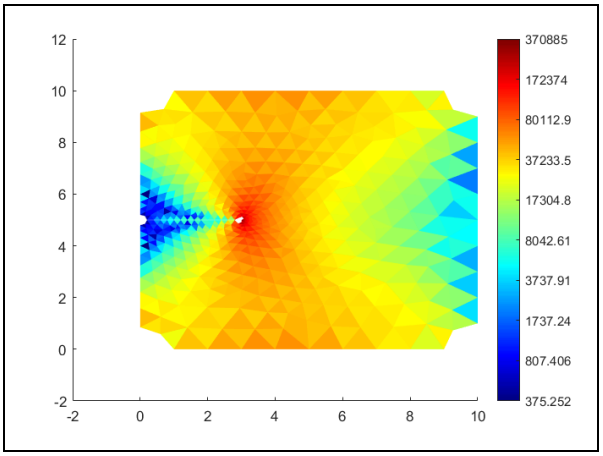

Figure 17: Semicircular crack modelling with a medium count of CSTs

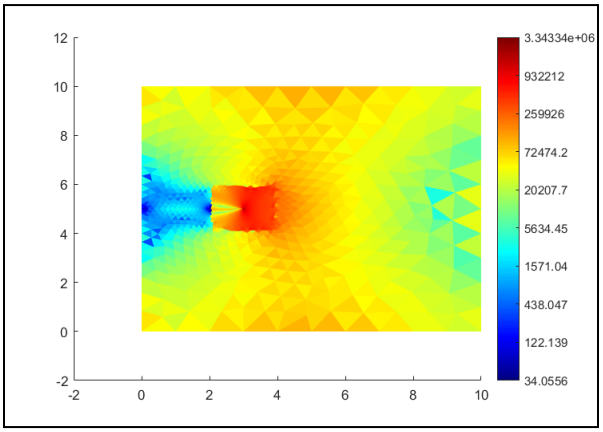

Figure 18: Composite crack for E = 10^2, ν = 0.1, box size = 2x2

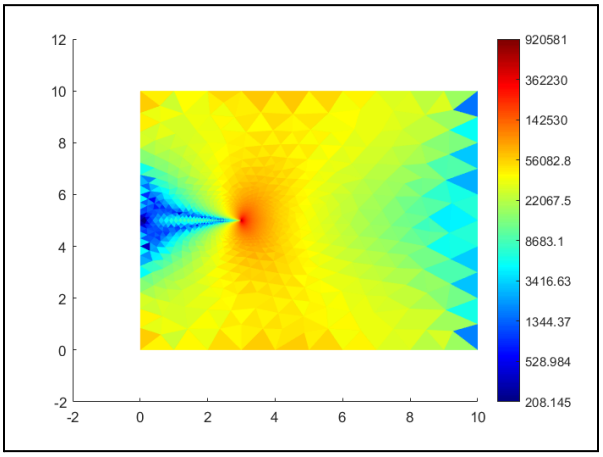

Figure 19: Composite crack for E = 10^{11}, ν = 0.0, box size = 2x2

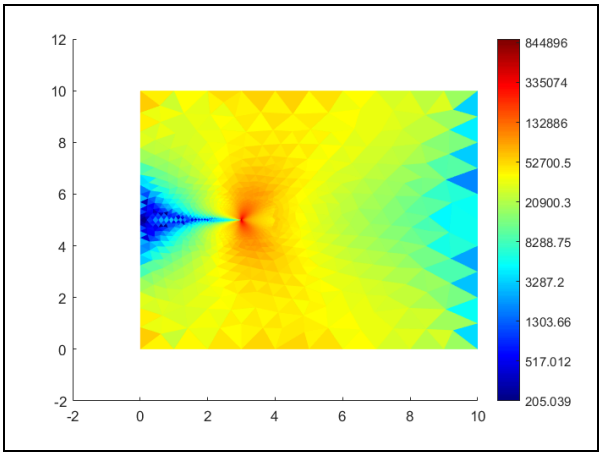

Figure 20: Composite crack for E = 10^{11}, ν = 0.5, box size = 2x2